Nanoscale

PAPER

View Article Online
View Journal | View Issue

Cite this: *Nanoscale*, 2020, **12**, 20506

Multiple d–d bonds between early transition metals in TM_2Li_n (TM = Sc, Ti) superatomic molecule clusters†

Yichun Zhou, Xinlei Yu and Longjiu Cheng *

Received 23rd July 2020,
Accepted 21st September 2020

DOI: 10.1039/d0nr05480a

rsc.li/nanoscale

The synthesis and application of compounds with Cr–Cr and V–V d–d quintuple bonds (σ, 2π, 2δ) have led to new thinking about whether d–d multiple bonds also exist between early transition metals such as Sc–Sc and Ti–Ti. In this study, by extensive unbiased global search at the density functional theory level, the low-energy structures of 26e and 30e TM_2Li_n clusters were obtained. Based on the super valence bond (SVB) theory, the prolate double-core structure of TM_2Li_n clusters was regarded as a superatomic molecule, of which each half was regarded as an open-shell superatom, and the electronic shell-closure was realized by forming multiple bonds between superatoms. Then, the quintuple super bonds (2δ, 2π, σ) of the $Li_{18}Ti_2$, $Li_{20}Sc_2$, $[Li_{17}V_2]^+$, $[Li_{17}Ti_2]^-$ clusters and the triple super bonds (2π, σ) of the $Li_{24}Sc_2$ and $Li_{24}Y_2$ clusters were confirmed *via* chemical-bonding analysis. This way of forming multiple bonds between early transition metals through superatomic bonding has promoted the experimental synthesis and application of early transition metal multiple bond compounds.

1 Introduction

Due to electronic characteristics and unique chemical properties, some transition metals with multiple bonds aroused widespread concern.[1–11] The synthesis of stable compounds with Cr–Cr quintuple bonds (σ, 2π, 2δ) in 2005 opened the door to metal–metal multiple bonds in the field of chemistry.[12–15] In recent years, the clusters and compounds with Mn–Mn triple bond and Mo–Mo quintet bond have been studied by both theoretical calculations and experiments.[16–22] A theoretical study found that the binuclear vanadium carbonyl compound $V_2(CO)_8$ consists of two $V(CO)_4$ units linked by a V–V quintuple bond.[23,24] The main group element boron is able to form multiple bonds with transition metals as revealed by quantum chemical investigation and identified by spectroscopy.[25–27] With the rapid increase in metal–metal bonding species, chemical bonding and electron properties were better understood because those substances were applied to numerous important fields such as catalysis and pharmaceutical chemistry.[28–31] In general, it is difficult for early transition metals to form electronic shell-closures by forming multiple bonds due to low number of d electrons such as Ti and Sc atoms, which are mostly present in ligand-protected compounds as single or double bonds.[32–38]

Compared with ligand-protected metal-bonded compounds, metal clusters tend to exhibit a variety of bonding methods in cluster science. The delocalized bonds formed in the metal clusters were usually explained by the jellium model,[39,40] which holds that the whole cluster be regarded as a superatom (SA) as well as the proper Aufbau rules is $|1S^2|1P^6|1D^{10}2S^2|1F^{14}2P^6|$ of the electron layer in the SA were different from those of the atom, and same as the magic number 2, 8, 20, 40..., observed on the mass spectrum.[41,42] Khanna, Jena and Castleman proposed that the metal clusters of magic numbers can be thought of as SAs, considering the stability and chemical similarity between simple metal clusters and individual atoms.[43–47] In 2013, the theory of the super valence bond (SVB) was proposed to explain the electron stability of Li_n clusters (Li_8, Li_{10}, Li_{14}), of which metal clusters can simulate the behavior of simple molecules in electronic shells.[48] The stability of non-spherical clusters was well explained using the SVB model, which was similar to a simple diatomic molecule, and realized the electronic shell-closure by the formation of super-multiple bonds between two SAs.[49–57] Based on this model, the as-synthesized ligand-protected Au_2Ag_{42} and Au_2Ag_{48} clusters are analogous to a Ne atom dimer (Ne_2).[58] The study of cluster bonding is helpful to develop the two-dimensional periodic table into the three-dimensional one.[59–64]

In our previous studies, it was found that the 26e Li_{26} and $Li_{20}Mg_3$ clusters, and 30e $Li_{18}Mg_3Al_2$ adopted double icosahe-

Department of Chemistry, Key Laboratory of Functional Inorganic Materials of Anhui Province, Anhui University Hefei, Anhui 230601, P. R. China. E-mail: clj@ustc.edu

†Electronic supplementary information (ESI) available. See DOI: 10.1039/d0nr05480a

dral structures, which can be seen as superatomic molecules with quintuple super bonds.[56] Similarly, the electronic properties of the tubular Au_{26} cluster revealed the cage–cage SA structure pattern, and the electron shell-closed of the cluster was realized by forming a triple super bond (σ, 2π) between the two cages.[50] The discovery of superatomic molecules with multiple bonds provides new ideas for the generation of d–d multiple bonds between early transition metals. We hope that Li atoms form a sealed cage on the outer layers of the early transition metals, and valence layer electrons are contributing to form multiple bonds between the early transition metals, thereby achieving an electronic shell-closed. Due to the 26e and 30e magic numbers observed in the mass spectrum of alkali metal clusters,[40] the superatomic molecules with 26e and 30e form multiple bonds to achieve an electronic shell-closure. Therefore, we first obtained stable 26e and 30e TM_2Li_n clusters through extensive unbiased global search combining the genetic algorithm (GA) with density functional theory (DFT). In order to verify that early transition metals formed multiple bonds in superatomic molecules, chemical-bonding analysis and electron localized functional (ELF) analysis will be discussed in the following section.

2 Computational method

The global optimal structures of TM_2Li_n clusters were obtained from more than 1000 times sampling optimization of each cluster by genetic algorithm (GA) combined with density functional theory (DFT), which is a powerful method for predicting the lowest energy structure of clusters.[65–67] In the global search, different spin multiplicities (m = 1 and 3) were considered. All structures were fully optimized at the PBE0/def2TZVP[68–70] level of theory and verified as true minima by frequency check. The adaptive natural density partition (AdNDP) method was used to perform the cluster-bonding analysis, which was invented by Boldyrev and can well analyze the delocalization of a multi-center bond.[71] The electronic localization functional (ELF)[72,73] analysis was drawn with Multiwfn.[74] The Wiberg bond index (WBI)[75] bond order (PBE0/def2TZVP) was also given by Multiwfn. All calculations in this paper were completed in the Gaussian 09 sequence package,[76] and the results were visualized using the MOLEKEL 5.4 program.[77]

3 Results and discussion

3.1 Geometric structures

Fig. 1 shows the low-energy isomers of $Li_{18}Ti_2$ (**A1–A4**), $Li_{20}Sc_2$ (**B1–B4**), $Li_{24}Sc_2$ (**C1–C3**), and $Li_{24}Y_2$ (**D1–D3**) clusters optimized at the PBE0/def2TZVP level of theory located by the extensive unbiased global search. The results of the global search agree with our expectations, where TM_2Li_n clusters are prolate double-core structures. The four isomers (**A1–A4**) of the $Li_{18}Ti_2$ cluster of 26e have considerable HOMO–LUMO energy

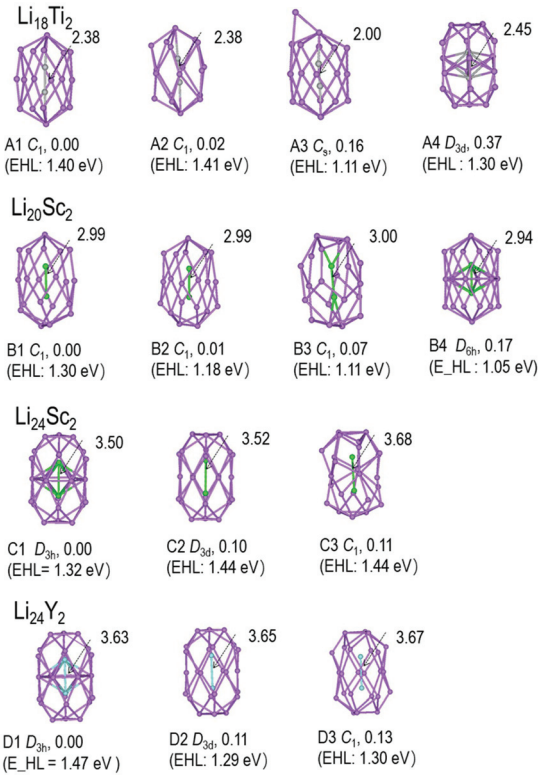

Fig. 1 Optimized lowest energy isomers of $Li_{18}Ti_2$ (**A1–A4**), $Li_{20}Sc_2$ (**B1–B4**) and $Li_{24}Sc_2$ (**C1–C3**), $Li_{24}Y_2$ (**D1–D3**) clusters at the PBE0/def2TZVP level of theory. Purple, blue, grey and green circles represent Li, Y, Ti and Sc, respectively. Bond lengths of TM–TM are given in Å.

gaps. The isomer (**A4**) was 0.37 eV higher than **A1** in energy. We believe that **A4** not only has a similar geometric configuration as **A1** but also has the same electronic structure. Similarly, the four isomers (**B1–B4**) of the $Li_{20}Sc_2$ clusters of prolate double-core structures have large HOMO–LUMO energy gaps. The isomer **B4** is 0.17 eV higher than **B1** in energy. $Li_{24}Sc_2$ clusters have 30 valence electrons, where the lowest-energy one (**C1**) has a high D_{3h} symmetry and a considerable energy gap (E_{HL} = 1.47 eV). Isomer **C2** (D_{3d}, E_{HL} = 1.44 eV), which is a rotational isomer of **C1**, is only 0.1 eV higher in energy than **C1**. Y is an atom of the same main group as Sc, and the geometric symmetry of the lowest-energy $Li_{24}Y_2$ (**D1**) cluster is also D_{3h} (E_{HL} = 1.47 eV).

3.2 $Li_{18}Ti_2$ and $Li_{20}Sc_2$

First, we discuss the electronic properties of $Li_{18}Ti_2$ and $Li_{20}Sc_2$ clusters with 26 valence electrons. It can be seen in Fig. 1 that the first four isomers of $Li_{18}Ti_2$ (**A1–A4**) have very similar geometric structures, which should also have similar electronic configurations. As shown in Fig. 2a, the canonical molecular orbital (MO) diagrams of **A1** and **A4** are very similar. **A4** has a higher D_{3d} symmetry than **A1**, and it is clearer from the MO analysis using **A4**. The prolate double-cage structure (**A4**) can be regarded as a combination of two Li_9Ti SA, which is open-shell based on the jellium model: $[1S^21P^6](1D2S)^5$.

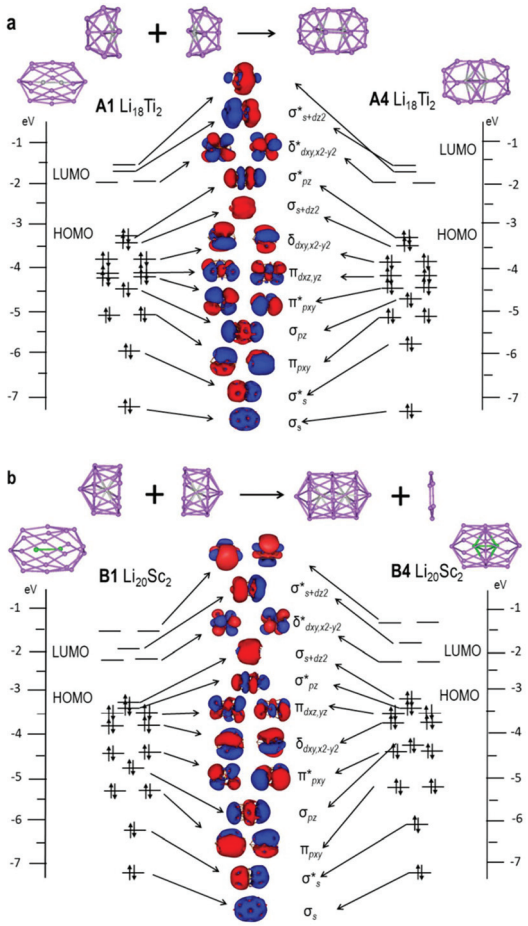

Fig. 2 Comparison of the Kohn–Sham MO diagrams of (a) $Li_{18}Ti_2$ (**A1** and **A4**) cluster and (b) $Li_{20}Sc_2$ (**B1** and **B4**) cluster (PBE0/def2-TZVP).

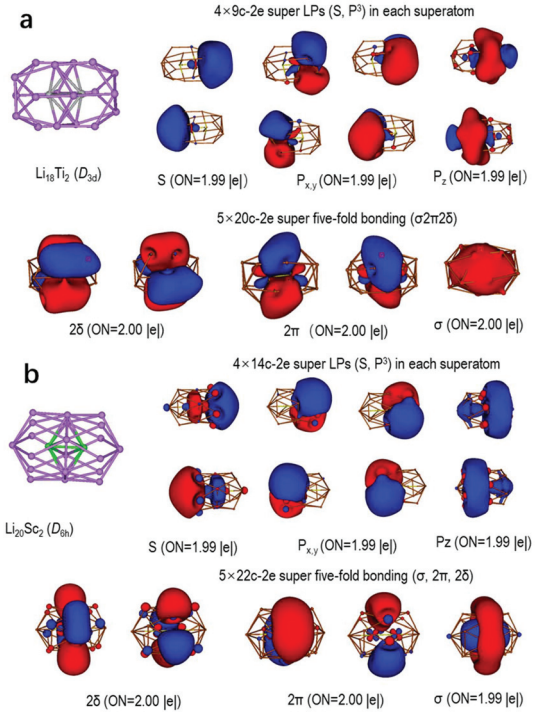

Fig. 3 Structures and AdNDP localized natural bonding orbitals of the (a) $Li_{18}Ti_2$ and (c) $Li_{20}Sc_2$ clusters. ON gives the occupancy numbers.

Then, the molecule-like electronic shell-closure can be realized through two Li_9Ti SAs $[8e](1D2S)^5$-$(1D2S)^5[8e]$ quintuple super bonds. From the MO diagrams, the valence MOs of the cluster can be viewed as four bonding orbitals (σ_s, $2\pi_{p_x,p_y}$, σ_{p_z}) and four anti-bonding orbitals (σ^*_s, $2\pi^*_{p_x,p_y}$, $\sigma^*_{p_z}$) correspond to the lone electron pair of each Li_9Ti SA ($1S^21P^6$). The remaining five occupied bonding orbitals were two double degenerate $\delta_{d_{xy,x^2-y^2}}$ orbitals, two degenerate $\pi_{d_{xz,yz}}$ orbitals, and a hybrid $\sigma_{s+d_{z^2}}$ orbital. There is a fairly large HOMO–LUMO gap from $\sigma^*_{p_z}$ to $\delta^*_{d_{xy,x^2-y^2}}$ (1.30 eV), resulting in a stable electronic structure of the superatomic molecule. Similarly, the $Li_{20}Sc_2$ cluster can be considered as a combination of two $Li_{13}Sc$ superatoms and share the nucleus of Li_6. Fig. 2b compares the MO diagrams of 26e $Li_{20}Sc_2$ (**B1** and **B4**) clusters, where it can be seen that the electron configuration and orbital shape of **B4** and **B1** are identical. $Li_{20}Sc_2$ is very similar to $Li_{18}Ti_2$ in MO diagrams, except for the energy level interleaving of two orbitals ($\delta_{d_{xy,x^2-y^2}}$ and $\pi_{d_{xz,yz}}$).

The chemical bonding analysis of AdNDP provides more direct evidence for the SA–SA bond, which further confirms our conclusion about the molecular orbital diagram. Fig. 3a depicts the AdNDP-bonding analysis of the $Li_{18}Ti_2$ superatomic molecule cluster. The results show that there are four 10c–2e lone pairs (SP^3) on each Li_9Ti SA. The five 20c–2e delocalization bonds, consist of one σ hybrid bond orbital of 2S + D_{z^2}, two degenerate π-bonding orbitals formed by D_{xz}–D_{xz} and D_{yz}–D_{yz} interactions, and then the mutual effect of D_{xy}–D_{xy} and $D_{x^2-y^2}$–$D_{x^2-y^2}$ constitute two double-degenerate δ-bonds. The chemical bonding analysis shown in Fig. 3b reveals that $Li_{20}Sc_2$ also has four 14c–2e super LPs in each $Li_{13}Sc$ SA ($1S^21P^6$) and five 22c–2e delocalization bonds (σ, 2π, 2δ).

In $Li_{18}Ti_2$ and $Li_{20}Sc_2$ clusters, the symmetry of the atomic d-orbital of Sc and Ti matches the superatomic orbital in forming the superatomic quintuple bonds (σ, 2π, 2δ). On the other hand, Ti–Ti and Sc–Sc bonds also display quintuple bonding characters. However, in Sc_7 and Ti_7 clusters, it does not have a clear superatom symmetry but behaves in a similar fashion to the states formed from atomic d-orbitals.[78]

3.3 $Li_{24}Sc_2$ and $Li_{24}Y_2$

Then, the electronic properties of the 30e $Li_{24}Sc_2$ and $Li_{24}Y_2$ clusters are discussed. $Li_{24}Sc_2$ and $Li_{24}Y_2$ clusters have the same geometric structure, which can be regarded as a combination of two $Li_{15}TM$ SAs sharing the nucleus of the middle Li_6. The $Li_{24}Y_2$ cluster should be consistent with the $Li_{24}Sc_2$ cluster in electronic configuration and orbital shapes. The MO diagrams of $Li_{24}Sc_2$ and $Li_{24}Y_2$ clusters are shown in Fig. 4, which can be viewed as six bonding orbitals (σ_s, $2\pi_{p_{xy}}$, σ_{p_z}, $2\delta_{d_{xy,x^2-y^2}}$) and six antibonding orbitals (σ^*_s, $2\pi^*_{p_{xy}}$, $\sigma^*_{p_z}$, $2\delta^*_{d_{xy,x^2-y^2}}$), corresponding to the super lone pairs of each SA. The remaining three occupied bonding orbitals are two degen-

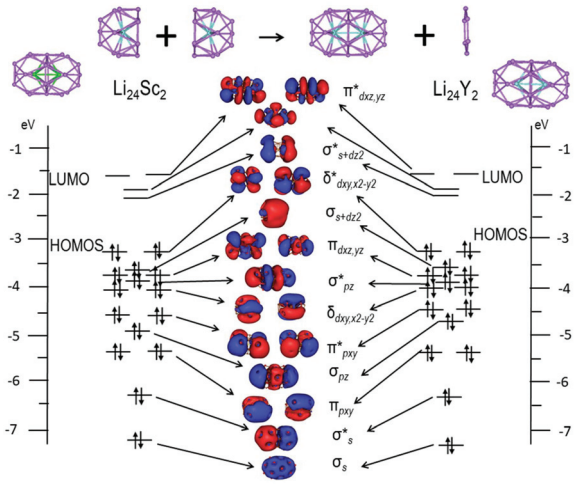

Fig. 4 Comparison of the Kohn–Sham MO diagrams of the $Li_{24}Sc_2$ and $Li_{24}Y_2$ clusters (PBE0/def2-TZVP).

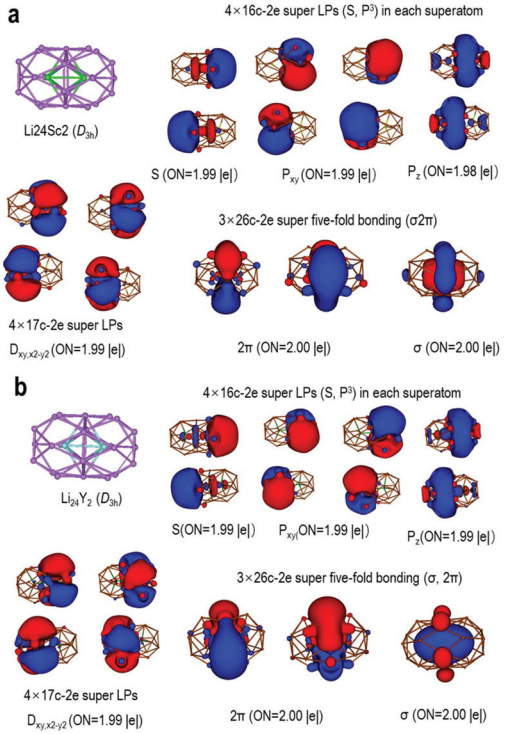

Fig. 5 Structures and AdNDP localized natural bonding orbitals of the (a) $Li_{24}Sc_2$ and (b) $Li_{24}Y_2$ clusters.

erate $\pi_{d_{xz,yz}}$ orbitals and one hybrid $\sigma_{s+d_{z^2}}$ orbital. Compared with the other 30e clusters, it is found that the $Li_{18}Mg_3Al_2$ cluster has a quintuple super bond (σ, 2π, 2δ),[56] and $Au_{24}In_2$ clusters have a triple super bond (σ, 2π).[50] However, the σ-bonding orbital in the $Au_{24}In_2$ cluster is a D_{z^2} orbital, whereas it is $\sigma_{s+d_{z^2}}$ orbital in $Li_{24}Sc_2$ and $Li_{24}Y_2$ clusters.

To verify the triple super bonds of $Li_{24}Sc_2$ and $Li_{24}Y_2$ clusters observed in MO diagrams, the AdNDP-bonding analysis was also performed. Fig. 5a shows the bonding analysis of the $Li_{24}Sc_2$ cluster, revealing that there are six 16c–2e lone pairs on each $Li_{15}Sc_2$ SA. The three 26c–2e delocalized bonds (σ, 2π) consisted of one $\sigma_{s+d_{z^2}}$ bond and two π-bonding orbitals (D_{xz}, and D_{yz}). The AdNDP chemical bonding of the $Li_{24}Y_2$ cluster (Fig. 5b) is exactly the same as in the $Li_{24}Sc_2$ cluster.

3.4 $Li_{17}V_2^+$ and $Li_{17}Ti_2^-$

It can be seen in Fig. 1 that the geometric structure of the lowest-energy isomer of $Li_{18}Ti_2$ cluster (**A1**) is not so good (in **C1** symmetry). However, the **A3** isomer can be seen as a perfect double icosahedral $[Li_{17}Ti_2]^-$ plus one additional Li^+ cationic atom. It is known that besides the electronic shell-closure, geometry is also a key factor in the stability of clusters. Thus, the $[Li_{17}Ti_2]^-$ cluster should be a magic number superatomic anion in both geometric and electronic shells. As expected, $[Li_{17}Ti_2]^-$ cluster was verified to be a true local minimum structure without virtual frequency, which maintains the D_{5h} symmetry with a fairly large HOMO–LUMO gap of 1.23 eV after structural relaxation at the PBE0/def2TZVP level of theory. The double icosahedral $[Li_{17}Ti_2]^-$ cluster can be regarded as a combination of two $Li_{11}Ti$ SAs sharing the nucleus of the middle Li_5. It can be seen in Fig. 6 that AdNDP results reveal that there are six 16c–2e super lone pairs on each $Li_{11}Ti$ SA, corresponding to four bonding orbitals (σ_s, $2\pi_{p_{x,y}}$, σ_{p_z}) and four antibonding orbitals (σ^*_s, $2\pi^*_{p_{x,y}}$, $\sigma^*_{p_z}$) in MO diagrams. The remaining five occupied MOs (σ, 2π, 2δ) can be regarded as a

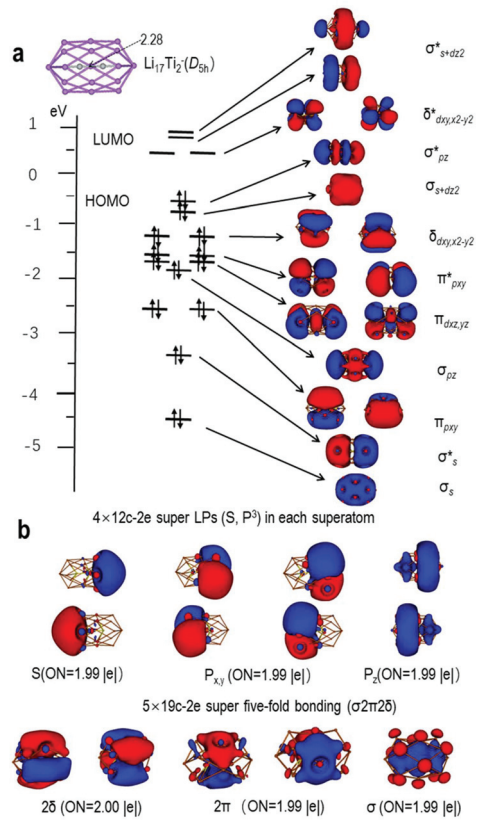

Fig. 6 MO diagrams (a) and AdNDP localized natural bonding orbitals (b) of the $Li_{17}Ti_2^-$ cluster. Bond lengths of TM–TM are given in Å.

19c–2e super quintuple bond delocalized over the entire cluster.

If we replace Ti by V, the $[Li_{17}V_2]^+$ cationic cluster also has 26 valence electrons. The double icosahedral $[Li_{17}V_2]^+$ cluster was also verified to be a true local minimum structure maintaining a D_{5h} symmetry, and it has a larger HOMO–LUMO gap of 1.38 eV. The V–V bond length in the $[Li_{17}V_2]^+$ cluster is only 1.75 Å, slightly longer than the length of typical quintuple V–V (1.69 Å)[56] and Cr–Cr (1.70 Å)[13] bonds. Similarly, the double icosahedral $[Li_{17}V_2]^+$ cluster can be regarded as a combination of two $Li_{11}V$ SAs sharing the nucleus of the middle Li_5. As can be seen from the MO diagrams in Fig. 7a, different from the case in the $[Li_{17}Ti_2]^-$ cluster, two π bonding and one σ bonding orbitals ($2\pi_{d_{xz,yz}}$, $\sigma_{s-d_{z^2}}$) are mainly localized on two V atoms, representing a direct V–V triple bond of d orbitals. The other six bonding orbits (σ_s, $2\pi_{p_{xy}}$, σ_{p_z}, $2\delta_{d_{xy,x^2-y^2}}$) and four antibonding orbitals (σ^*_s, $2\pi^*_{p_{xy}}$, $\sigma^*_{p_z}$) are delocalized on the entire cluster. Furthermore, the AdNDP-bonding analysis in Fig. 7b shows that the $[Li_{17}V_2]^+$ cluster contains four 12c–2e super (SP^3) lone pairs in each $Li_{11}V$ SA, and two 19c–2e delocalized superatomic bonds (2δ) as well as three localized V–V bonds (σ, 2π). From the difference between the bonding patterns of $[Li_{17}Ti_2]^-$ and $[Li_{17}V_2]^+$ clusters, it can be seen that V_2 favors more direct d–d multiple bonds, whereas the d–d multiple bonds between Ti_2 are more delocalized by a superatomic bond, resulting in a large gap in the TM–TM bond length.

ELF is an effective method for analyzing the electronic structures of clusters that shows the color and shape of the electron density distributed across the cross-section of the cluster, and has the advantages of a clear image and simple function form. To further confirm the quintuple bonds in the $[Li_{17}V_2]^+$ and $[Li_{17}Ti_2]^-$ clusters, Fig. 8 compares their ELF contour with the molecules with a quintuple atomic bond (V_2 and Cr_2F_2). Clearly, the superatomic clusters have very similar ELF contour of σ, π and δ orbits with the simple molecules, which further confirms the quintuple bonds between two superatoms in $[Li_{17}V_2]^+$ and $[Li_{17}Ti_2]^-$ clusters. The ELF analysis for $Li_{18}Ti_2$, $Li_{20}Sc_2$, $Li_{24}Sc_2$, and $Li_{24}Y_2$ clusters is given in ESI (Fig. S1 and S2†).

3.5 Effective bond order

The TM–TM bond lengths also agree with the super bond orders. The Sc–Sc bond length in the $Li_{24}Sc_2$ cluster (3.50 Å) with triple bonds is obviously longer than that of the $Li_{20}Sc_2$ cluster (2.94 Å) with quintuple bonds. However, as listed in Table 1, the TM–TM bond lengths are quite different in the clusters with quintuple bonds, which may be related to the degree of localization of the quintuple super bonds on TM_2. Thus, we calculate the occupation number localized on TM_2 of the quintuple super bond (Fig. S3†), and the effective bond order is defined as half of the total localized occupation numbers on TM_2. As shown in Table 1, the calculated effective bond orders are consistent with the WBI bond orders and the lengths of TM–TM. In particular, the WBI (4.35) and effective bond orders (4.46) of the $[Li_{17}V_2]^+$ cluster are close to 5. It further illustrates that in superatomic molecule clusters Sc and Ti atoms tend to form delocalized multi-center bonds, whereas V atoms tend to form localized V–V bonds. For comparison, the bond order and bond lengths of Ti_2, Sc_2, and V_2 molecules are also listed in Table 1 (MO diagrams of Ti_2, Sc_2, and V_2

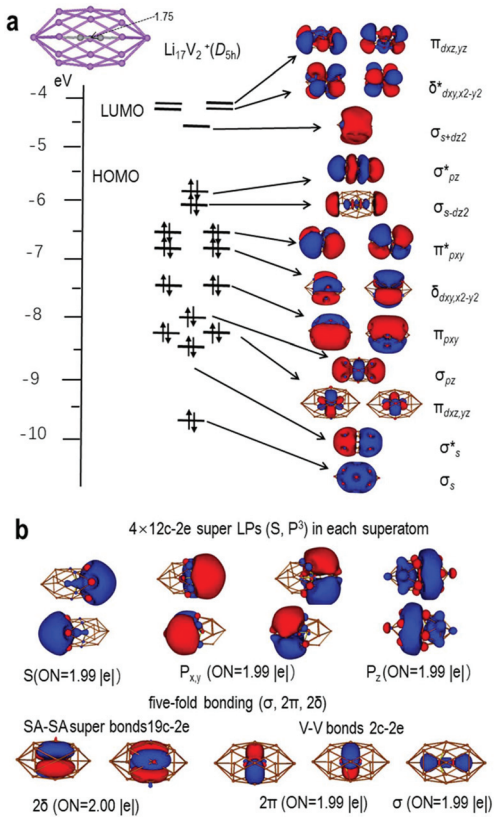

Fig. 7 MO diagrams (a) and AdNDP localized natural bonding orbitals (b) of the $Li_{17}V_2^+$ cluster. Bond lengths of TM–TM are given in Å.

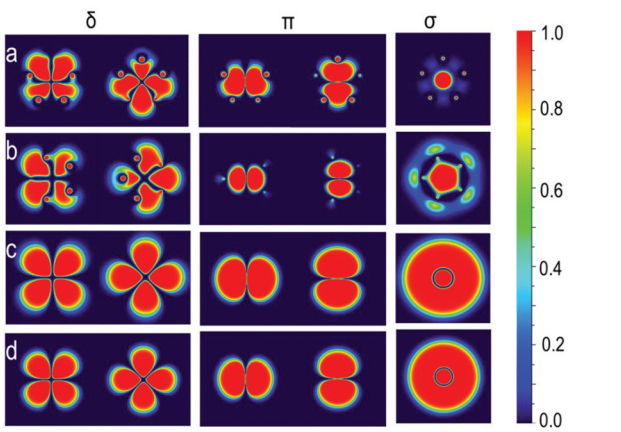

Fig. 8 ELFs of quintuple bonding $[Li_{17}V_2]^+$ (a), $[Li_{17}Ti_2]^-$ (b), V_2 (c) and Cr_2F_2 (d) in color and shape. The scale is labeled aside. All cross-sections are perpendicular to the double transition metal. ELF values are between 0 (no localization, blue) and 1 (complete localization, red).

Table 1 Comparison of bond order, Wiberg bond indices, effective bond order and TM–TM bond lengths (Å) for $Li_{24}Sc_2$ (**C1**), $Li_{20}Sc_2$ (**B4**), $Li_{18}Ti_2$ (**A4**), $[Li_{17}Ti_2]^-$, $[Li_{17}V_2]^+$ clusters and V_2, Ti_2, Sc_2 molecules

	$Li_{24}Sc_2$	$Li_{20}Sc_2$	$Li_{18}Ti_2$	$[Li_{17}Ti_2]^-$	$[Li_{17}V_2]^+$	V_2	Ti_2	Sc_2
Bond order	3	5	5	5	5	5	4	2
WBI bond order	0.52	1.18	1.86	2.3	4.35	5.97	4.93	2.83
Effective bond order	1.61	2.60	3.15	3.93	4.46			
Bond length	3.50	2.94	2.45	2.28	1.75	1.69	1.86	2.55

molecules are given in ESI†). The V–V distance in the $[Li_{17}V_2]^+$ cluster (1.75 Å) is very close to that in the V_2 molecule (1.69 Å). However, Sc–Sc (Ti–Ti) distances in superatomic molecule clusters are obviously longer than those in Sc_2 (Ti_2) molecules, although the former one has higher bond orders. Thus, it is better to take the Sc–Sc and Ti–Ti bonds in superatomic molecule clusters as chemical bonds displaying quintuple/triple bonding characters.

4 Conclusions

In summary, by extensive unbiased global search at the DFT level, the global optimal geometric structure of $Li_{24}Y_2$, $Li_{24}Sc_2$, $Li_{18}Ti_2$ and $Li_{20}Sc_2$ clusters were located. All the structures were verified to be stable minima with high HOMO–LUMO gaps and without imaginary frequency. AdNDP chemical-bonding analysis shows that $Li_{18}Ti_2$ and $Li_{20}Sc_2$ have quintuple bonds (σ, 2π, 2δ), while $Li_{24}Y_2$ and $Li_{24}Sc_2$ form triple bonds (σ, 2π). In addition, two D_{5h} double icosahedral clusters, $[Li_{17}Ti_2]^-$ and $[Li_{17}V_2]^+$, are also very stable with high HOMO–LUMO gaps, of which quintuple bonds (σ, 2π, 2δ) were also verified. The TM–TM bond lengths agree with the super bond orders, where the Sc–Sc bond length in the $Li_{24}Sc_2$ cluster (3.50 Å) with triple bonds is obviously longer than that of the $Li_{20}Sc_2$ cluster (2.94 Å) with quintuple bonds. In the $[Li_{17}V_2]^+$ cluster, three bonds (σ, 2π) are totally localized on V_2, whereas two δ bonds are delocalized over the whole cluster. This leads to a highly effective bond order of V_2, resulting in a very short V–V bond length (very close to the value in V_2 molecule). The TM–TM bond lengths also agree well with the effective bond orders in the clusters with quintuple bonding characters ($Li_{20}Sc_2$, $Li_{18}Ti_2$, $[Li_{17}Ti_2]^-$ and $[Li_{17}V_2]^+$). This study gives a further understanding of the metal–metal multiple bonding between early transition metals, which may provide a new reference for the experimental synthesis.

Conflicts of interest

There are no conflicts of interest to declare.

Acknowledgements

This work is financed by the National Natural Science Foundation of China (21873001), and by the Foundation of Distinguished Young Scientists of Anhui Province. The calculations were carried out at the High-Performance Computing Center of Anhui University.

References

1 Y. Chen and S. Sakaki, *Dalton Trans.*, 2014, **43**, 11478–11492.
2 L. Kang, Z. Sun, L. Meng and X. Li, *Chem. Phys. Lett.*, 2019, **731**, 136600.
3 M. Brynda, L. Gagliardi, P. O. Widmark, P. P. Power and B. O. Roos, *Angew. Chem., Int. Ed.*, 2006, **45**, 3804–3807.
4 B. O. Roos, A. C. Borin and L. Gagliardi, *Angew. Chem., Int. Ed.*, 2007, **46**, 1469–1472.
5 U. Radius and F. Breher, *Angew. Chem., Int. Ed.*, 2006, **45**, 3006–3010.
6 X. Zhai, G. Li, Q. S. Li, Y. Xie, R. B. King and H. F. Schaefer, *J. Phys. Chem. A*, 2011, **115**, 3133–3143.
7 L. Gagliardi and B. O. Roos, *Nature*, 2005, **433**, 848–851.
8 D. L. Lichtenberger, C. D. Ray, F. Stepniak, Y. Chen and J. H. Weaver, *J. Am. Chem. Soc.*, 1992, **114**, 10492–10497.
9 W. Klotzbuecher and G. A. Ozin, *Inorg. Chem.*, 1977, **16**, 984–987.
10 X. Wang and L. Andrews, *J. Phys. Chem. A*, 2004, **108**, 11006–11013.
11 B. Xu, Q. S. Li, Y. Xie, R. B. King and H. F. Schaefer, *J. Phys. Chem. A*, 2009, **113**, 12470–12477.
12 J. Joy and E. D. Jemmis, *Chem. Commun.*, 2017, **53**, 8168–8171.
13 A. Falceto, K. H. Theopold and S. Alvarez, *Inorg. Chem.*, 2015, **54**, 10966–10977.
14 T. Nguyen, A. D. Sutton, M. Brynda, J. C. Fettinger and P. P. Power, *Science*, 2005, **310**, 844–847.
15 R. H. Duncan Lyngdoh, H. F. Schaefer and R. B. King, *Chem. Rev.*, 2018, **118**, 11626–11706.
16 T. Jian, L. F. Cheung, J. Czekner, T. T. Chen, G. V. Lopez, W. L. Li and L. S. Wang, *Chem. Sci.*, 2017, **8**, 7528–7536.
17 T. Alonso-Lanza, J. W. González, F. Aguilera-Granja and A. Ayuela, *J. Phys. Chem. C*, 2017, **121**, 25554–25560.
18 H. W. Chen, S. Mallick, S. F. Zou, M. Meng and C. Y. Liu, *Inorg. Chem.*, 2018, **57**, 7455–7467.
19 Y. Chen and S. Sakaki, *Inorg. Chem.*, 2017, **56**, 4011–4020.
20 J. K. Bao, Z. T. Tang, H. J. Jung, J. Y. Liu, Y. Liu, L. Li, Y. K. Li, Z. A. Xu, C. M. Feng and H. Chen, *J. Am. Chem. Soc.*, 2018, **140**, 4391–4400.

21 H. Cho, K. Hong, M. L. Strader, J. H. Lee and T. K. Kim, *Inorg. Chem.*, 2016, **55**, 5895–5903.
22 R. Helge, L. J. Andreas, C. C. Wilder, S. Walter, S. V. Ackerbauer, M. B. Gamza and G. Yuri, *Proc. Natl. Acad. Sci. U. S. A.*, 2018, **115**, 7706–7710.
23 R. B. King, H. F. Schaefer, Z. Liu, Q. S. Li and Y. Xie, *J. Organomet. Chem.*, 2008, **693**, 1502–1509.
24 O. Hubner and H. J. Himmel, *Angew. Chem.*, 2020, **59**, 2–9.
25 C. Chi, J. Q. Wang, H. S. Hu, Y. Y. Zhang, W. L. Li, L. Meng, M. Luo, M. Zhou and J. Li, *Nat. Commun.*, 2019, **10**, 4713.
26 L. F. Cheung, T. T. Chen, G. S. Kocheril, W. J. Chen, J. Czekner and L. S. Wang, *J. Phys. Chem. Lett.*, 2020, **11**, 659–663.
27 T. T. Chen, L. F. Cheung, W. J. Chen, J. Cavanagh and L. S. Wang, *Angew. Chem.*, 2020, **59**, 15260–15265.
28 Y. S. Huang, G. T. Huang, Y. L. Liu, J. S. K. Yu and Y. C. Tsai, *Angew. Chem., Int. Ed.*, 2017, **56**, 15427–15431.
29 L. Andrews and H.-G. Cho, *Angew. Chem.*, 2019, **59**, 2496–2504.
30 L. X. Kang, Z. Sun, L. P. Meng and X. Y. Li, *Chem. Phys. Lett.*, 2019, **731**, 136600.
31 F. A. Cotton, E. A. Hillard and C. A. Murillo, *J. Am. Chem. Soc.*, 2003, **125**, 2026–2027.
32 X. Zhang, Q. S. Li, Y. Xie, R. B. King and H. F. Schaefer, *Inorg. Chem.*, 2010, **49**, 1961–1975.
33 X. Yan, X. Li, Z. Sun, Q. Li and L. Meng, *New J. Chem.*, 2016, **40**, 1988–1996.
34 A. F. Kilpatrick, J. C. Green, F. G. Cloke and N. Tsoureas, *Chem. Commun.*, 2013, **49**, 9434–9436.
35 A. F. Kilpatrick, J. C. Green and F. G. Cloke, *Organometallics*, 2015, **34**, 4816–4829.
36 A. Ovchinnikov and S. Bobev, *Inorg. Chem.*, 2019, **58**, 2934–2941.
37 F. G. N. Cloke, J. C. Green, A. F. R. Kilpatrick and D. O'Hare, *Coord. Chem. Rev.*, 2017, **344**, 238–262.
38 H.-G. Xu, Z.-G. Zhang, Y. Feng and W. Zheng, *Chem. Phys. Lett.*, 2010, **498**, 22–26.
39 K. E. Schriver, J. L. Persson, E. C. Honea and R. L. Whetten, *Phys. Rev. Lett.*, 1990, **64**, 2539–2542.
40 W. A. D. Heer, *Rev. Mod. Phys.*, 1993, **65**, 611–676.
41 V. Y. Shevchenko and A. E. Madison, *Glass Phys. Chem.*, 2002, **28**, 40–43.
42 B. Sven and B. Jrn, *Philos. Mag.*, 1999, **79**, 1321–1342.
43 S. N. Khanna and P. Jena, *Phys. Rev. B: Condens. Matter Mater. Phys.*, 1995, **51**, 13705–13716.
44 D. E. Bergeron, *Science*, 2004, **304**, 84–87.
45 A. c. Reber, S. N. Khanna, A. Castleman and J. Welford, *J. Am. Chem. Soc.*, 2007, **129**, 10189–10194.
46 L. Cheng, Y. Yuan, X. Zhang and J. Yang, *Angew. Chem., Int. Ed.*, 2013, **52**, 9035–9039.
47 D. E. Bergeron, P. J. Roach, A. W. Castleman, N. O. Jones and S. N. Khanna, *Science*, 2005, **307**, 231–235.
48 L. Cheng and J. Yang, *J. Chem. Phys.*, 2013, **138**, 141101.
49 L. Yuan, L. Cheng and J. Yang, *J. Phys. Chem. C*, 2015, **119**, 23274–23278.
50 Q. Liu, C. Xu, X. Wu and L. Cheng, *Nanoscale*, 2019, **11**, 13227–13232.
51 L. Yan, *J. Phys. Chem. A*, 2019, **123**, 5517–5524.
52 A. Munoz-Castro, *Chem. Commun.*, 2019, **55**, 7307–7310.
53 T. Dainese, S. Antonello, S. Bogialli, W. Fei, A. Venzo and F. Maran, *ACS Nano*, 2018, **12**, 7057–7066.
54 L. Cheng, C. Ren, X. Zhang and J. Yang, *Nanoscale*, 2013, **5**, 1475–1478.
55 L. Cheng, X. Zhang, B. Jin and J. Yang, *Nanoscale*, 2014, **6**, 12440–12444.
56 H. Wang and L. Cheng, *Nanoscale*, 2017, **9**, 13209–13213.
57 Q. Zheng, C. Xu, X. Wu and L. Cheng, *ACS Omega*, 2018, **3**, 14423–14430.
58 S. Jin, X. Zou, L. Xiong, W. Du, S. Wang, Y. Pei and M. Zhu, *Angew. Chem., Int. Ed.*, 2018, **57**, 16768–16772.
59 Q. Liu and L. Cheng, *J. Alloys Compd.*, 2019, **711**, 762–768.
60 S. Chen, S. Wang, J. Zhong, Y. Song and M. Zhu, *Angew. Chem., Int. Ed.*, 2015, **54**, 3145–3149.
61 P. Jena, *J. Phys. Chem. Lett.*, 2013, **4**, 1432–1442.
62 S. Giri, S. Behera and P. Jena, *J. Phys. Chem. A*, 2014, **118**, 638–645.
63 S. A. Claridge, A. Castleman, S. N. Khanna, C. B. Murray and P. S. Weiss, *ACS Nano*, 2009, **3**, 244–255.
64 G. Abbas, S. Zhao, Z. Li and J. Yang, *ACS Omega*, 2018, **3**, 11966–11971.
65 C. Roberts and R. L. Johnston, *Phys. Chem. Chem. Phys.*, 2001, **3**, 5024–5034.
66 B. Hartke, *Iran. J. Public Health*, 1993, **97**, 9973–9976.
67 R. L. Johnston, *Dalton Trans.*, 2003, 4193–4207.
68 C. Adamo and V. Barone, *J. Chem. Phys.*, 1999, **110**, 6158–6170.
69 J. M. D. Campo, J. L. Gazquez, S. B. Trickey and A. Vela, *J. Chem. Phys.*, 2012, **136**, 104108–104108.
70 F. Weigend and R. Ahlrichs, *Phys. Chem. Chem. Phys.*, 2005, **7**, 3297–3305.
71 D. Y. Zubarev and A. I. Boldyrev, *Phys. Chem. Chem. Phys.*, 2008, **10**, 5207–5017.
72 A. Savin, R. Nesper, S. Wengert and T. F. Fassler, *Angew. Chem., Int. Ed. Engl.*, 1997, **36**, 1808–1832.
73 J. K. Burdett and T. A. Mccormick, *J. Phys. Chem. A*, 1998, **102**, 6366–6372.
74 T. Lu and F. Chen, *J. Comput. Chem.*, 2012, **33**, 580–592.
75 K. B. Wiberg and P. R. Rablen, *J. Comput. Chem.*, 1993, **14**, 1504–1518.
76 M. Frisch, G. Trucks, H. Schlegel, G. Scuseria, M. Robb, J. Cheeseman, G. Scalmani, V. Barone, B. Mennucci and G. Petersson, *Gaussion 09*, Gaussian, Inc., CT, 2010.
77 U. M. Varetto, *Version 5.4. 0.8*, Swiss National Supercomputing Centre, Manno, Switzerland, 2009.
78 J. T. A. Gilmour and N. Gaston, *Phys. Chem. Chem. Phys.*, 2019, **21**, 8035–8045.

